Inclinometer Monitoring of the Castelrotto Landslide in Italy

Lucia Simeoni[1] and Luigi Mongiovì[2]

Abstract: Over the last decades the real-time displacement monitoring systems have been increasingly used for assessing the risk conditions due to landslide movements and for managing the early-warning systems. Any decision about safety actions is therefore based upon the data provided by the instrumentation. The purpose of this work is to suggest how in-place inclinometers may be combined with periodical measurements by using a mobile probe in order to evaluate the current movement of a landslide and to assess the reliability of data. The monitoring system installed at the landslide of Castelrotto (northern Italy) is described, giving some details on the instrumentation and the data collected so far. A local quadratic trend model is developed to estimate the kinematic characteristics of the movement, and a statistical procedure for comparing real-time data with periodical measures is given to assess the reliability of data. This analysis shows how the direction of the displacement may be used as an indicator of reliability.

DOI: 10.1061/(ASCE)1090-0241(2007)133:6(653)

CE Database subject headings: Landslides; Displacement; Monitoring; Reliability; Italy.

Introduction

Since 1997 the University of Trento has been charged from the A22-Brenner Highway Board with the study of the stability of the slope comprised between 64+500 and 65+500 km of the highway. The site was investigated by drilling ten boreholes, and equipping them with seven inclinometer casings and eight piezometric cells of Casagrande type. Water level and inclinometer measurements have been performing periodically. They have revealed the existence of a 2.5×10^6 m^3 slide, which in conjunction with extreme rainfall events moves along a well-defined sliding surface. So far the maximum average rate of displacement has been about 1.5 cm in 6 months.

Although movements have been small—classifying the landslide as an extremely slow landslide (Cruden and Varnes 1994), a potential risk of a general collapse, and the catastrophic consequences of such a slide due to the filling of the narrow Isarco Valley cannot be ignored. Accordingly, the A22 Highway Board requested the real-time monitoring of the displacements in order to estimate the kinematic characteristics of the movement and to assess the risk condition by defining a landslide displacement evolution model. In January 2001 an automatic monitoring system was therefore installed for measuring the landslide movements. It consists of seven vertical in-place inclinometers and a raingage connected to an automatic data acquisition system with a wireless communication device.

[1]Research Fellow, Dept. of Mechanical and Structural Engineering, Univ. of Trento, via Mesiano, 77, 38050 Trento, Italy. E-mail: lucia.simeoni@ing.unitn.it

[2]Full Professor, Dept. of Mechanical and Structural Engineering, Univ. of Trento, via Mesiano, 77, 38050 Trento, Italy. E-mail: mongiovi@ing.unitn.it

Note. Discussion open until November 1, 2007. Separate discussions must be submitted for individual papers. To extend the closing date by one month, a written request must be filed with the ASCE Managing Editor. The manuscript for this paper was submitted for review and possible publication on June 15, 2005; approved on December 18, 2006. This paper is part of the ***Journal of Geotechnical and Geoenvironmental Engineering***, Vol. 133, No. 6, June 1, 2007. ©ASCE, ISSN 1090-0241/2007/6-653–666/$25.00.

To date, the major role of the University of Trento has been to define data processing procedures in order to check the reliability of measurements and to evaluate the kinematic characteristics of the slide movements correctly. In fact, series of data are affected by errors due to the irregular sensor performance, shortcomings at the system architecture, as well as disturbances due to the performance of manual measurements. Particular procedures are then needed to take these errors into account.

Landslide

The study area is approximately triangular in shape (Fig. 1) with two sides bordered by rocky scarps of ignimbrite and the third one by the Isarco River. The area is located in the Isarco Valley, a left tributary of the Adige River, 20 km north of Bolzano (Trentino-Alto Adige Region, northern Italy). This valley represents one of the most important communication ways between south and north Europe: it accommodates the A22-Brenner Highway, the railway and the 12-State Road that link Italy with Austria through the Brenner pass.

In 1997 ten boreholes (Fig. 2) were drilled in the lower part of the triangular area. Seven boreholes (S1, S2, S4, S8, S9, S11, and S12) were equipped by inclinometer casings and three by eight piezometric cells of Casagrande type (S6, S7, and S10). Further, three boreholes (T8, T11, and T12) were drilled in the late 2000 and equipped with inclinometer casings to substitute Inclinometers S8, S11, and S12 no longer usable. In 2004 Inclinometer T12 was substituted by the new Inclinometer V12.

The cross-section passing at Boreholes S4, S8, and S11 is shown in Fig. 3. The borings established the existence of a bedrock of tuff that is covered by debris consisting of blocks of tuff and ignimbrite set in a sandy to clayey matrix. The thickness of the upper deposit varies from 60 m at Borehole S2–23 m in the lower part of the slope. At the northwestern part of the slope (Boreholes S12, T12, S11, and T11) a layer of recent alluvial deposit Al was identified between the tuff and the debris. Accordingly, it is likely that the mass of debris moved downward to the valley, and covered the alluvial deposit. The mass of debris has a

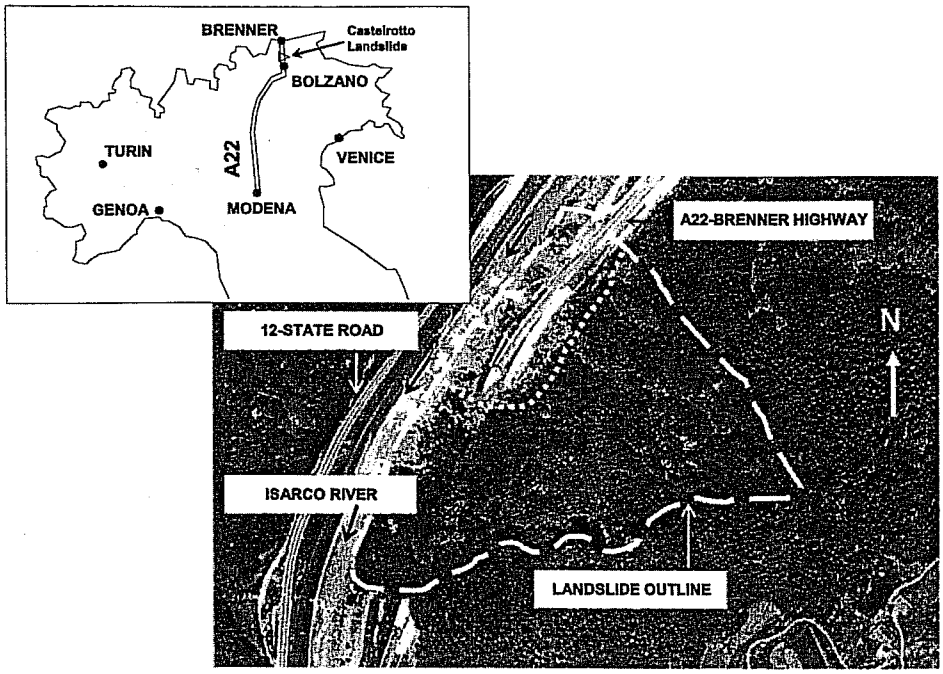

Fig. 1. Location map and general setting of the landslide area. The area bordered by the dotted line was excavated during the highway construction.

volume of approximately 2.5×10^6 m^3 and occupies an area of about 100,000 m^2.

Periodical Monitoring of Displacements

In order to gain some insight into the kinematics of the slope, deep displacements have been periodically measured since 1997 by using a mobile inclinometer probe, whose characteristics are reported in Table 1. During the first year the measurements were carried out every month, while later they were performed four to five times per year.

Local inclinometer displacements have clearly revealed the existence of a major sliding surface located at the bottom of the debris (Fig. 3) and dipping of about 20°. In Fig. 4 an example of cumulative displacements are shown for Inclinometer S4: the major sliding surface is located approximately at 36 m depth, and a minor sliding surface formed in late 2000 at 15 m depth.

Cumulative displacements on a 150 cm thick sliding zone are displayed in Fig. 5(a) for each inclinometer. It is seen that displacements measured at the inclinometers located in the northern part of the landslide (S4, S8, T8, S11, T11, and S12) are generally higher in magnitude than those measured in the southern one (S2, S1, and S9). Besides, the directions of the first group of

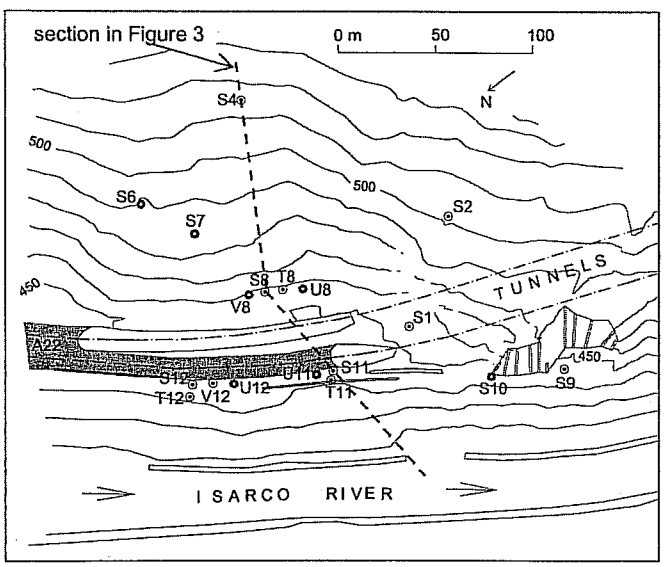

Fig. 2. Borehole positions. Boreholes S1, S2, S4, S8, T8, S9, S11, S12, T12, and V12 are equipped with Inclinometers, S6, S7, S10, U8, V8, U11, and U12 with piezometers. Inclinometers S8, S11, S12, and T12 are no longer used.

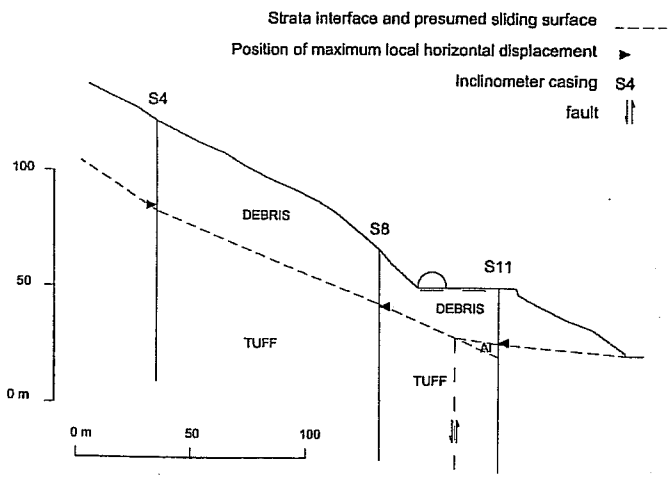

Fig. 3. Cross section passing at Boreholes S4, S8, and S11

Table 1. Datasheet of the Mobile and In-Place Inclinometer Probes (after Sisgeo S.r.l.)

Probe type	Mobile	In-place
Distance between wheel axes (mm)	500	1,000
Sensor type	biaxial servo-accelerometer	biaxial servo-accelerometer
Sensor range	±30°	±30°
Sensor resolution	±0.005 mm per 500 mm	0.001% full scale
Accuracy	±4.00 mm per 30 m	0.05% full scale

displacements range from 293 to 322° clockwise from the north direction, whereas direction of the second group ranges from 275 to 285° [Fig. 5(b)]. For example, at Inclinometer S4 a total displacement at the sliding zone of 4.5 cm toward 293° has been calculated so far, while at Inclinometer S9 it assumes a value of 0.9 cm toward 283°. The maximum amount of displacement has been of about 1.5 cm in 6 months (at Inclinometer S4 from December 2000 to June 2001).

By comparing the cumulative local displacements to rainfall it has also been recognized that the landslide reactivates during the rainy seasons. No direct correlations between movement and rainfall has been possible to find so far; therefore, the study of hydraulic model that takes the whole meteorological history (both rainfall and evapotranspiration) and the real unsaturated nature of the soil into account is in progress.

Real-Time Monitoring of Displacements

Inadequate knowledge concerning the pore pressure distribution within the landslide in addition to soil shear strength parameters is currently insufficient to design the remedial works or to forecast the landslide movements. Besides, the movements evaluated from the periodical monitoring are averaged over the interval between two measurements, and therefore the estimate of their kinematic characteristic may be misleading as they are mean values (Bhandari 1988). With this information it cannot be denied that sudden or accelerated movements could take place, causing the displacements to reach unacceptable levels at the surface.

Owing to this potential risk or to a general collapse of the slope causing a break in the road as well as the filling of the narrow Isarco Valley, the A22 Highway Board requested a real-time knowledge of the landslide displacements so that in the event of movement accelerations vehicle access could be prohibited. For this purpose, in January 2001 an automatic monitoring system was installed for measuring the landslide movements and studying a landslide displacement evolution model. This model should connect the expected displacements with the meteorological history. When the evolution model is defined devices capable of stopping the traffic, e.g., gates or stop lights, will be installed.

The monitoring system consists of seven in-place inclinometers fixed in seven different inclinometer casings, a data acquisition unit, a wireless communicating device and a personal computer (Fig. 6). In-place inclinometers were installed in the same casings where measurements have been periodically carried out by using the mobile inclinometer probe. Only one in-place inclinometer probe was installed in each tube because a well-defined sliding zone was recognized by performing the periodical measurements.

As the architecture of the system and the characteristics of each component may influence the pattern of the series of measures and the data processing procedure, a detailed description of them is given in the following.

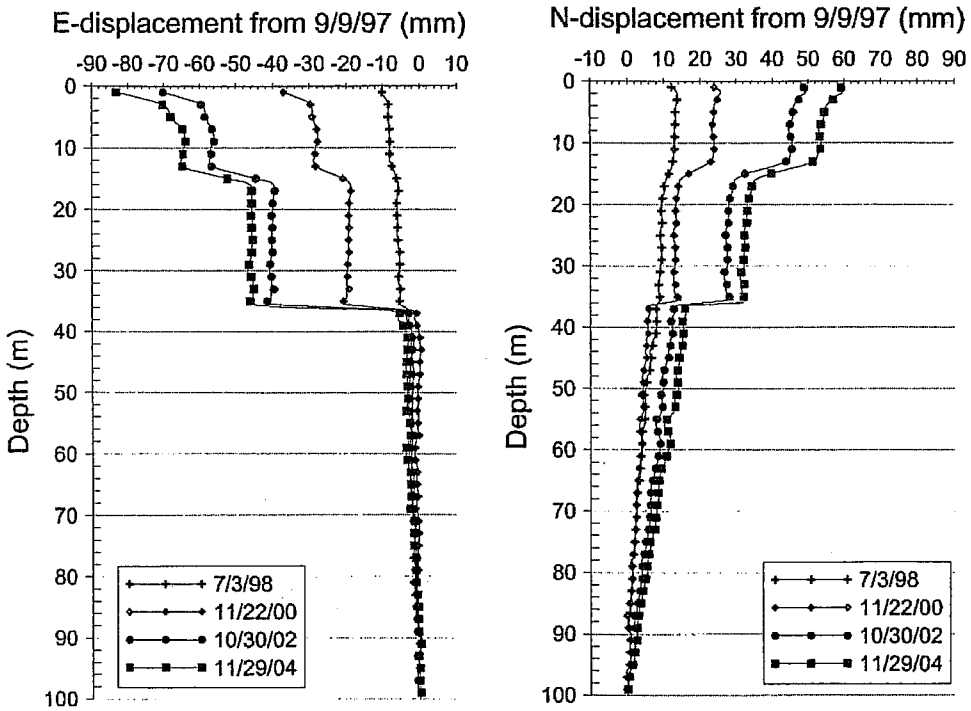

Fig. 4. Cumulative displacements (E=eastern component and N=northern component) at Inclinometer S4 revealing two sliding surfaces: the major one is located at 36 m depth and the minor at 15 m

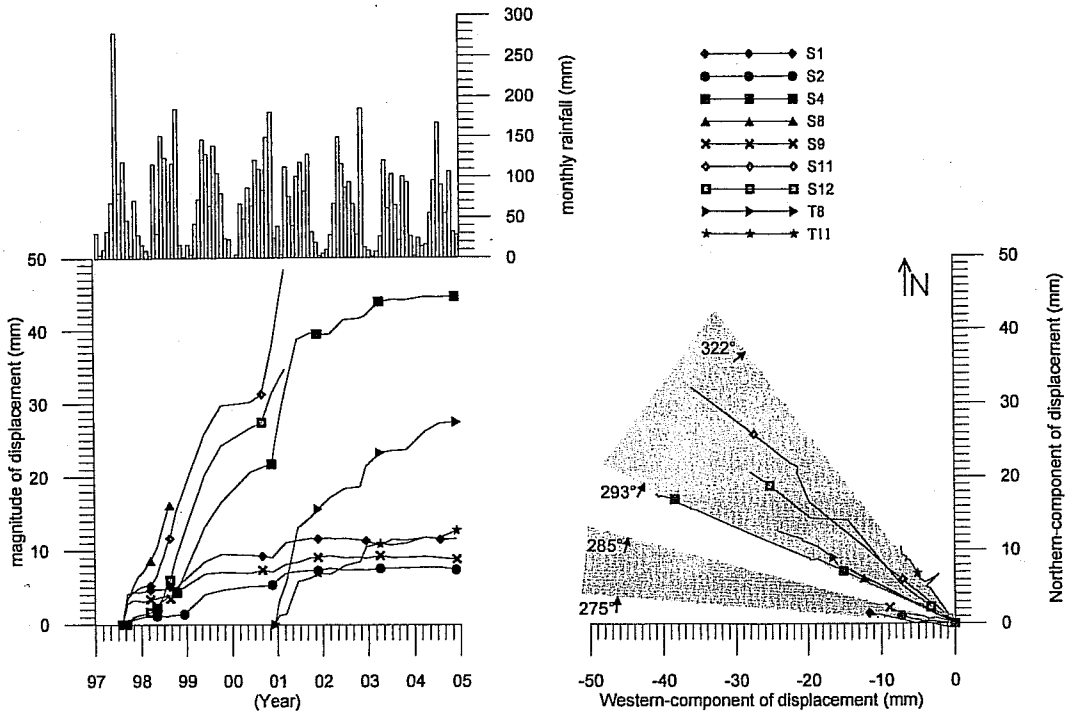

Fig. 5. Displacements calculated at the sliding surface: (a) displacement magnitudes versus time; (b) directions; and (c) monthly rainfall

In-Place Inclinometers

The probes are equipped with the biaxial sensors of servo-accelerometer type whose characteristics are reported in Table 1. They are powered by a ±12 V_{dc} and their output is ±5,000 mV. According to the data in Table 1, resolution and accuracy may be expressed as 0.0006° ≅ 0.05 mV and 0.03° ≅ 2.5 mV or, by taking into account the distance between wheels of 1,000 mm, as 0.01 and 0.26 mm, respectively.

Calibration of sensors was performed in the factory by tilting the probes at fixed inclinations in the full range ±30° and measuring the electrical values. The maximum differences between calibration curves and calibration measures resulted equal to 0.39 mm by assuming a linear regression, and to 0.21 mm by assuming a cubic polynomial curve.

The inclinometer probes were placed at the depth of the sliding surface (ranging from 23 m at Inclinometer T11 to 64 m at Inclinometer S2), by hanging them on the top head with an invar cable. In this way, the location of the probe can be varied by shortening or lengthening the wire.

Data Acquisition Unit

The data acquisition unit consists of a fully programmable Campbell Scientific CR10X datalogger, with nonvolatile memory and a battery backed clock. The specifications of this datalogger are: Analog input range of ±2,500 mV (half of the range of probe sensors); resolution 0.333 mV (effective resolution of 13.9 bits); accuracy ±5 mV in the temperature range from −25 to 50°C. An electrically erasable programmable read only memory of 2 Mb stores the operated system, user programs, and data.

The CR10X is powered by a 12 V_{dc} connected to the power line and stabilized by an external battery. An internal lithium battery enables the datalogger program and the stored data to remain in memory and also allows the clock to continue to keep time when power is disconnected. As the monitoring system was installed, data have been collected at 15 min intervals. Analog input of sensors are acquired in a differential mode after a warm-up of 15 s. Prior to March 2002 an amplifier divided the analog signals by two in order to fit the full scale range of sensors (±5,000 mV) to the full scale range of the data acquisition system (±2,500 mV). Digital output was then doubled via software. On March 25, 2002 the amplifier was removed and the analog signal was no longer reduced for the reason that will be better explained later. Sensor measurements, time, voltage of battery power, and temperature of datalogger are recorded.

The data acquisition unit is connected to the sensors by a multiplexer for switching the signal to each sensor, and by seven power supply cards, which transform the 12 into ±12 V_{dc}. A stabilized voltage signal of about 235 mV is also connected to the multiplexer in order to detect any disturbance to the A/D conversion and communication.

Communication and Data Collection

Communication of data have been performed by means of a remote GSM modem connected to the CR10X by a serial port and

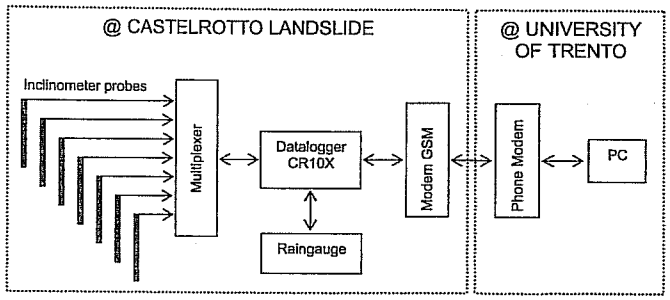

Fig. 6. Architecture of the real-time monitoring system

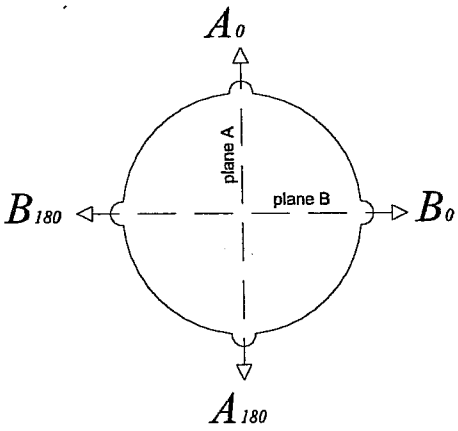

Fig. 7. Standard inclinometer casing nomenclature

two phone modems located at the University of Trento and at the Highway Board. Downloading and data collection are made through the Multilogger Software by Canary System. Multilogger is used for managing the downloading, data collection, terminal emulation, text, and graphical monitoring. It also provides an editor for modifying setup files, instruction files, or the downloading file.

Multilogger also provides facilities for managing an early warning system by presetting the relevant thresholds. However, since the purpose of the system has only been the monitoring, those facilities have not been used.

Major Problems with the Instrumentation

In addition to the amplifier, problems have also been encountered with the probes and the dc/dc converters. So far two inclinometer probes suddenly stopped working and were substituted; three times one dc/dc converter was damaged by a lightning strike and another time a dc/dc converter changed its output and the system started providing unreliable measures.

Processing of Mobile Inclinometer Data

Mobile and in-place inclinometer measurements have been processed in order to define the kinematic characteristics of the landslide movements. Mobile inclinometer data have been processed with the aim to define the changes of the casing profiles with respect to time and, therefore, to evaluate the horizontal displacements that occurred at different vertical positions inside the landslide mass. As vectors, with magnitudes and directions (Cooper 2000), the displacements are able to provide the right information on the kinematic of the landslide only if directions have been evaluated correctly. If this is the case, it is possible, for example, to establish whether the landslide moves as a whole toward the same direction or it is a complex slide with components moving toward different directions.

For the purpose of calculating the direction of displacements correctly, groove spiral measurements of the casing tubes were initially performed, and an average spiral rotation of nearly 1°/m clockwise was obtained. Because the sliding surface was identified at depths ranging between 23 and 60 m, a maximum relative rotation of the movement directions of about 37° would be expected due to the spiral. Nevertheless a subsequent accurate calibration of the spiral probe revealed that 1°/m corresponds to the

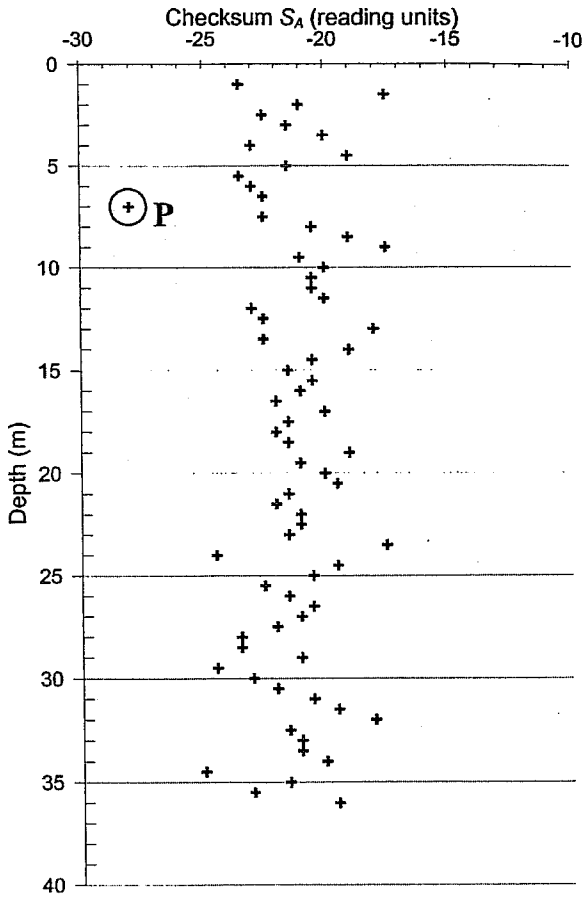

Fig. 8. Checksum S_A for Measurement 27 (October 2, 2001) in Casing T8

offset of the sensor, and therefore the spiral rotation of grooves has to be neglected in the processing of the readings.

Attention has been paid to the evaluation of the reliability of the inclinometer measures by rejecting the readings with gross errors and estimating the accuracy of the horizontal displacements. This approach was found to be very useful to evaluate the significance of displacements when they were extremely small in magnitude and to compare those displacements to the ones calculated from the in-place inclinometer measurements.

Standard readings (Dunnicliff 1993; ASTM D 4622-86) taken in the opposite directions A_0 and A_{180} on plane A, B_0, and B_{180} on plane B (Fig. 7) may be expressed as

$$A_0 = A + \varepsilon^s_{A0} + \varepsilon^r_{A0} \tag{1a}$$

$$B_0 = B + \varepsilon^s_{B0} + \varepsilon^r_{B0} \tag{1b}$$

$$A_{180} = -A + \varepsilon^s_{A180} + \varepsilon^r_{A180} \tag{1c}$$

$$B_{180} = -B + \varepsilon^s_{B180} + \varepsilon^r_{B180} \tag{1d}$$

where A and B=true values on planes A and B (deterministic); ε^s_{Ai} and ε^s_{Bi}=systematic errors on planes A and B (deterministic); ε^r_{Ai} and ε^r_{Bi}=random errors on planes A and B, respectively (normally distributed and assumed to be independent).

Differences $\bar{A}$ and $\bar{B}$ of readings on planes A and B and checksums S_A and S_B are given by

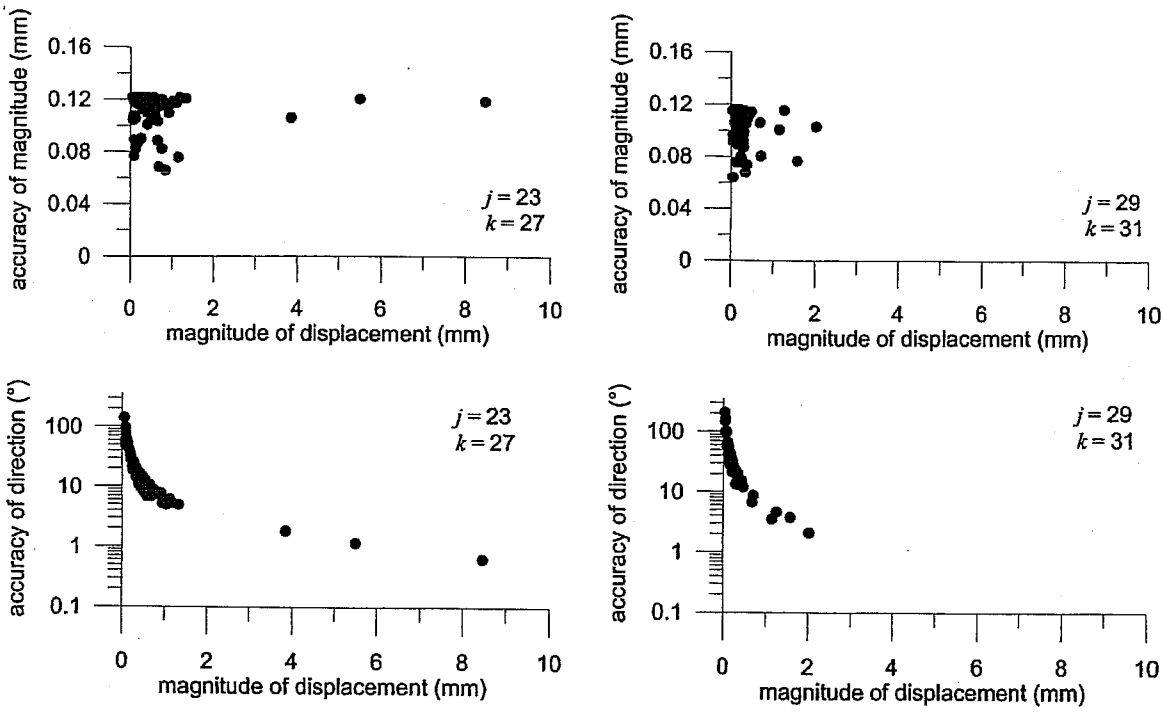

Fig. 9. Accuracies of magnitude and direction of displacements from Readings 23–27 and 29–31

$$\bar{A} = \frac{A_0 - A_{180}}{2} = A + \frac{\varepsilon^s_{A0} - \varepsilon^s_{A180}}{2} + \frac{\varepsilon^r_{A0} - \varepsilon^r_{A180}}{2} \tag{2a}$$

$$\bar{B} = \frac{B_0 - B_{180}}{2} = B + \frac{\varepsilon^s_{B0} - \varepsilon^s_{B180}}{2} + \frac{\varepsilon^r_{B0} - \varepsilon^r_{B180}}{2} \tag{2b}$$

$$S_A = \frac{A_0 + A_{180}}{2} = \frac{\varepsilon^s_{A0} + \varepsilon^s_{A180}}{2} + \frac{\varepsilon^r_{A0} + \varepsilon^r_{A180}}{2} \tag{2c}$$

$$S_B = \frac{B_0 + B_{180}}{2} = \frac{\varepsilon^s_{B0} + \varepsilon^s_{B180}}{2} + \frac{\varepsilon^r_{B0} + \varepsilon^r_{B180}}{2} \tag{2d}$$

If systematic errors are due only to instruments bias (the small nonzero value the probe reads at vertical) and they do not change while measuring, i.e.

$$\varepsilon^s_{A0} = \varepsilon^s_{A180} \tag{3a}$$

$$\varepsilon^s_{B0} = \varepsilon^s_{B180} \tag{3b}$$

expressions (2) may be written as

$$\bar{A} = A + \varepsilon^{r(-)}_A \approx N(\hat{A}, \sigma^2_A) \tag{4a}$$

$$\bar{B} = B + \varepsilon^{r(-)}_B \approx N(\hat{B}, \sigma^2_B) \tag{4b}$$

$$S_A = \varepsilon^s_A + \varepsilon^{r(+)}_A \approx N(\hat{S}_A, \sigma^2_A) \tag{4c}$$

$$S_B = \varepsilon^s_B + \varepsilon^{r(+)}_B \approx N(\hat{S}_B, \sigma^2_B) \tag{4d}$$

Differences and checksums are normally distributed (verifiable by the Pearson's test) with equal variances on the same plane. Mean values of distributions are $\hat{A}$ and $\hat{B}$ for differences, and $\hat{S}_A$ and $\hat{S}_B$ for checksums.

Given the normal distributions of checksums, gross errors may be recognized by applying the Chauvenet criteria (Taylor 1986). For example, with reference to the values of checksum A reported in Fig. 8 for measurement No. 27 in the casing T8, we want to know if value S_{sus}=–28 reading units (point P) refers to a gross error. Mean and variance of checksum S_A are, respectively

$$\hat{S}_A = E(S_A) = \frac{1}{N}\sum_{i=1}^{N} S_{Ai} = -21.2 \tag{5}$$

$$s^2_A = E(\sigma^2_A) = \frac{1}{N-1}\sum_{i=1}^{N-1} (S_{Ai} - \hat{S}_A) = 3.4 \tag{6}$$

where i refers to the ith reading of the total number N=71.

According to Chauvenet criteria the suspected value S_{sus} will be affected by a gross error if the expected number n of $|S_A|$ bigger than $|S_{sus}|$ is less than 0.5. Let $P(|S_A| > |S_{sus}|)$ the probability of $|S_A| > |S_{sus}|$, the expected number n is

$$n = NP(|S_A| > |S_{sus}|) = 71 \times 0.00025 = 0.02 \tag{7}$$

Because n is less than 0.5, S_{sus} is rejected and supposed to include a gross error. New values of –21.1 reading units and of 2.8 square reading units are obtained for $\hat{S}_A$ and s^2_A by neglecting S_{sus} in Eqs. (5) and (6).

The recalculated values of s^2_A and s^2_B may be used as a measure of accuracy of readings and to estimate accuracy of displacements. If $\bar{A}_i|^k_j$ and $\bar{B}_i|^k_j$ are the changes of differences $\bar{A}$ and $\bar{B}$ at depth i calculated from readings collected during measurements j and k ($j<k$), the magnitude $d_i|^k_j$ and the direction $\vartheta_i|^k_j$ (clockwise from axes A_0) of displacement at depth i are given by

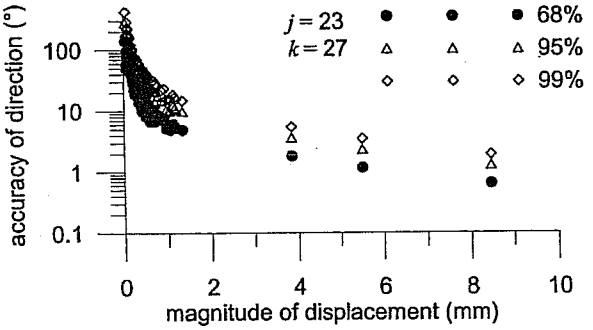

Fig. 10. Accuracy of direction for different multiples of the standard deviation

$$d_i|_j^k = D\sqrt{\left(\frac{\bar{B}_i|_j^k}{K_B}\right)^2 + \left(\frac{\bar{A}_i|_j^k}{K_A}\right)^2} \tag{8}$$

$$\vartheta_i|_j^k = 2\arctan\frac{\left(\frac{\bar{B}_i|_j^k}{K_B}\right)}{\sqrt{\left(\frac{\bar{B}_i|_j^k}{K_B}\right)^2 + \left(\frac{\bar{A}_i|_j^k}{K_A}\right)^2} + \left(\frac{\bar{A}_i|_j^k}{K_A}\right)} \tag{9}$$

where D=distance between the wheels of the probe and K_A and K_B=instrumental constants of sensor obtained from calibration.

As changes of differences are still normally distributed, their variances are given by

$$s_A^2|_j^k = s_{A_j}^2 + s_{A_k}^2 \tag{10a}$$

$$s_B^2|_j^k = s_{B_j}^2 + s_{B_k}^2 \tag{10b}$$

and may be used to estimate an upper bound for accuracy of displacement according to the general expressions valid for any variable distribution (Taylor 1986)

$$s_d|_j^k \leqslant \left|\frac{\partial d}{\partial \bar{A}}\right| s_A|_j^k + \left|\frac{\partial d}{\partial \bar{B}}\right| s_B|_j^k = \frac{D}{\sqrt{\left(\frac{\bar{B}_i|_j^k}{K_B}\right)^2 + \left(\frac{\bar{A}_i|_j^k}{K_A}\right)^2}} \times\left[|\bar{A}_i|_j^k|\frac{s_A|_j^k}{(K_A)^2} + |\bar{B}_i|_j^k|\frac{s_B|_j^k}{(K_B)^2}\right] \tag{11}$$

$$s_\vartheta|_j^k \leqslant \left|\frac{\partial \vartheta}{\partial \bar{A}}\right| s_A|_j^k + \left|\frac{\partial \vartheta}{\partial \bar{B}}\right| s_B|_j^k = \frac{1}{K_A K_B\left[\left(\frac{\bar{B}_i|_j^k}{K_B}\right)^2 + \left(\frac{\bar{A}_i|_j^k}{K_A}\right)^2\right]} \times[|-\bar{B}_i|_j^k|\, s_A|_j^k + |\bar{A}_i|_j^k|\, s_B|_j^k] \tag{12}$$

Standard deviation $s_A|_j^k$ has generally resulted of about 2.5 reading units, equivalent to 0.06 mm, whereas standard deviation $s_B|_j^k$ has been always larger than $s_A|_j^k$ and of about 4 reading units, equivalent to 0.10 mm.

When K_A=K_B=K, Eqs. (11) and (12) reduce to

$$s_d|_j^k \leqslant \frac{D}{K\sqrt{(\bar{B}_i|_j^k)^2 + (\bar{A}_i|_j^k)^2}}[|\bar{A}_i|_j^k|s_A|_j^k + |\bar{B}_i|_j^k|s_B|_j^k] = \frac{D}{d_i|_j^k K}[|\bar{A}_i|_j^k|s_A|_j^k + |\bar{B}_i|_j^k|s_B|_j^k] \tag{13}$$

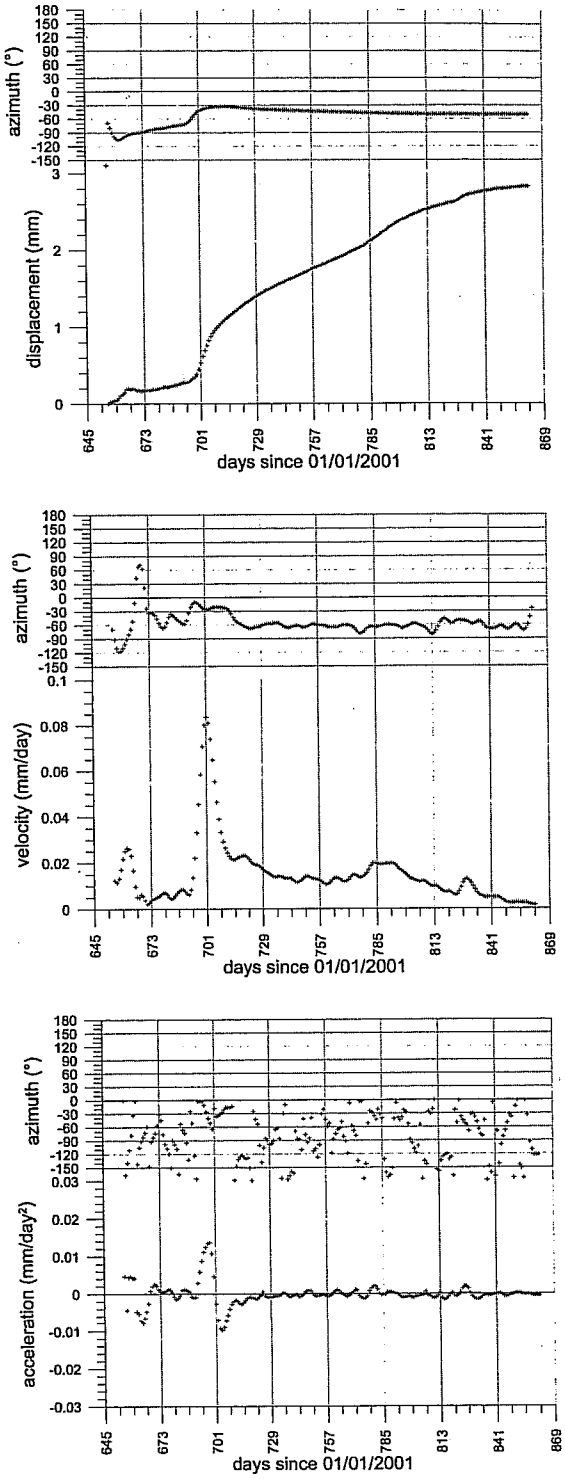

Fig. 11. Estimates of displacement, velocity, and acceleration from data of Inclinometer T8. Angles of azimuth are measured from north direction: clockwise between 0 and 180°, and anticlockwise between 0 and −180°

$$s_\vartheta|_j^k \leqslant \frac{1}{[(\bar{B}_i|_j^k)^2 + (\bar{A}_i|_j^k)^2]}[|-\bar{B}_i|_j^k|s_A|_j^k + |\bar{A}_i|_j^k|s_B|_j^k] = \left(\frac{D}{d_i|_j^k K}\right)^2[|-\bar{B}_i|_j^k|s_A|_j^k + |\bar{A}_i|_j^k|s_B|_j^k] \tag{14}$$

To see how the accuracy varies with reference to the magnitude of

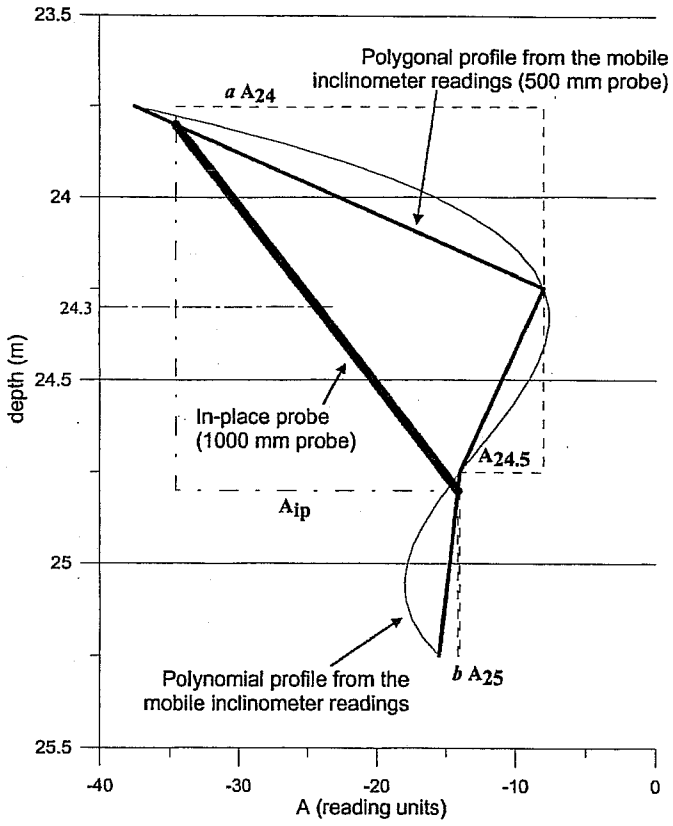

Fig. 12. Sketch of the profiles used for evaluating the optimal in-place inclinometer probe position and the reliability of displacements

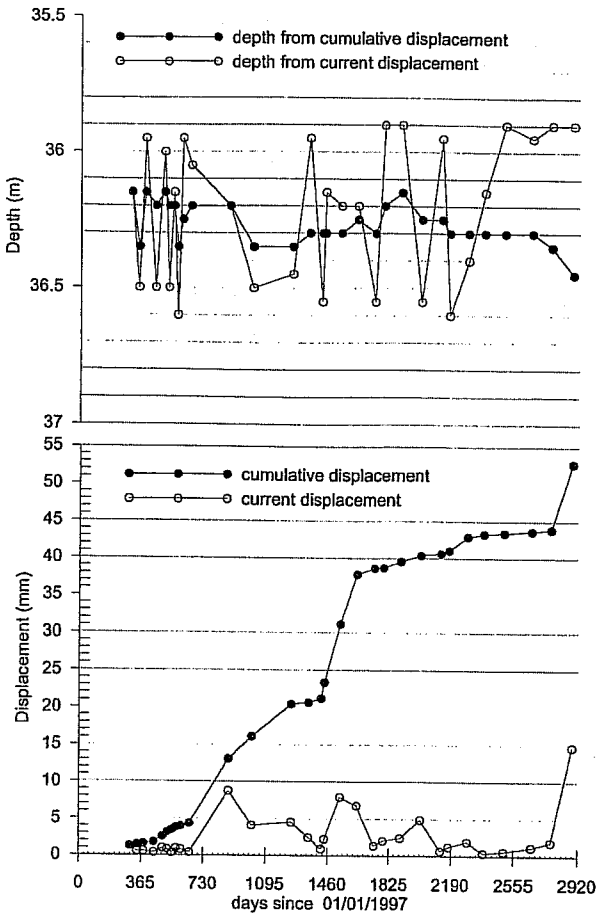

Fig. 13. Depth of maximum displacement in a 1,000 mm thick zone for Inclinometer S4

displacements, Fig. 9 reports the results for local displacements that occurred in between measurements 23 (December 14, 2000) and 27 (October 2, 2001), and in between measurements 29 (March 7, 2002) and 31 (June 3, 2002) in Casing T8. The instrumental constant K is equal to 20,000 reading units/sen (sen=sine of the angle of probe inclination) and the distance D=500 mm. It is seen that accuracy of magnitude ranges between 0.06 and 0.13 mm, independently of the magnitude of displacement, meanwhile accuracy of direction decreases as magnitude of displacement increases. This is consistent with expression (12) or expression (14), in which displacement is at ratio with power two. In particular, accuracy of less than 5° was obtained for local displacements bigger than 1 mm.

In Eqs. (11)–(14) the standard deviation of Readings A and B are taken as estimates of accuracy of the measures. According to the normal distribution function it corresponds to accepting only 68% of measures. Larger probability of 95 or 99% may be obtained by assuming accuracy of the measures equal to twice or three times the standard deviation, respectively. The accuracy of magnitude and direction of displacements also increases, making the maximum values of accuracy of magnitude of displacements equal to 0.24 mm for the 95% probability and 0.37 mm for the 99% probability. Fig. 10 shows the values of accuracy of the direction of displacements calculated with j=23 and k=27. This analysis has confirmed that bigger displacements (as large as 3–4 mm) are now needed to reduce the accuracy to values less than 5°.

Processing of In-Place Inclinometer Data

Data collected by the in-place inclinometer probes consist of two series of signals y_A and y_B, which are expressed as voltage measures and are related to the probe inclinations on Planes A and B perpendicular to each other. In order to use these data for managing an alert and alarm system, a processing method capable of estimating the kinematic characteristics of the movements has been defined. It is based on the time series analysis by applying a bivariate local quadratic trend model (LQTM) defined as

$$\mathbf{y}_t = \boldsymbol{\mu}_t + \boldsymbol{\lambda}\mathbf{x}_t + \mathbf{G}_t\boldsymbol{\varepsilon}_t$$

$$\boldsymbol{\mu}_t = \boldsymbol{\mu}_{t-1} + \boldsymbol{\beta}_t + \mathbf{D}_t\boldsymbol{\delta}_t$$

$$\boldsymbol{\beta}_t = \boldsymbol{\beta}_{t-1} + \boldsymbol{\gamma}_t + \mathbf{E}_t\boldsymbol{\zeta}_t$$

$$\boldsymbol{\gamma}_t = \boldsymbol{\gamma}_{t-1} + \mathbf{F}_t\boldsymbol{\xi}_t \qquad (15)$$

The first equation represents the measurement equation, and the other three equations are transition equations. $\mathbf{y}_t$=vector of observed variables y_A and y_B at time t; $\boldsymbol{\mu}_t$=trend component; $\boldsymbol{\beta}_t$ and $\boldsymbol{\gamma}_t$=slope components; $\boldsymbol{\varepsilon}_t$, $\boldsymbol{\delta}_t$, $\boldsymbol{\zeta}_t$, and $\boldsymbol{\xi}_t$=vectors of serially uncorrelated disturbances, normally distributed with means zero and covariance matrixes equal to the identity matrixes; $\mathbf{G}_t$, $\mathbf{D}_t$, $\mathbf{E}_t$, and $\mathbf{F}_t$=nonstochastic matrixes; and $\boldsymbol{\lambda}\cdot\mathbf{x}_t$ refers to the signal shift. $\boldsymbol{\mu}_t$, $\boldsymbol{\beta}_t$, and $\boldsymbol{\gamma}_t$ represent the so-called state vector and are related to displacement, velocity, and acceleration of the movement,

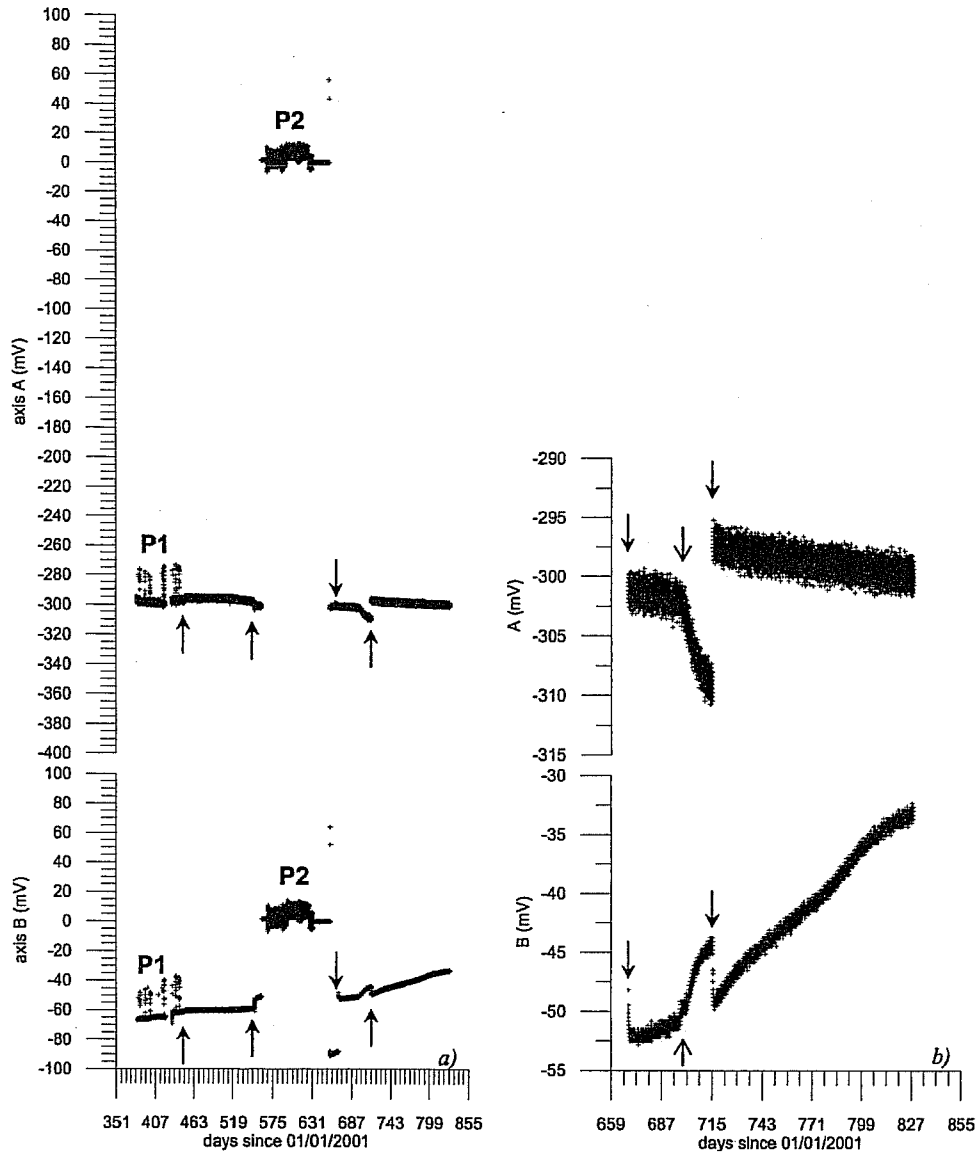

Fig. 14. (a) Data of Axes *A* and *B* recorded by the T8 inclinometer from January 15, 2002 (380 days after January 1, 2001) to April 8, 2003 (828); (b) enlargement from October 30, 2002 (668) to April 8, 2003 (828). Closed arrows point at the manual inclinometer measurements, open arrows point at a water level measurement.

respectively; $\boldsymbol{\lambda} \cdot \mathbf{x}_t$ introduces the shift of the signal occurring when the manual measurements are performed.

Given the two signals y_A and y_B, time series analysis has been performed by using the library of state space function SsfPack 2.2 by Koopman et al. (1999), linked to the object oriented matrix programming language Ox 2.3 of Doornik (1998). Details on the model and the data processing are reported in Simeoni et al. (2003). Once the matrixes $\mathbf{G}_t$, $\mathbf{D}_t$, $\mathbf{E}_t$, and $\mathbf{F}_t$ have been estimated by maximizing the log-likelihood function, the Kalman filter has been applied as a backward recursion in order to estimate the state vector $\boldsymbol{\mu}_t$, $\boldsymbol{\beta}_t$ and $\boldsymbol{\gamma}_t$.

Vectors of displacement, velocity, and acceleration obtained by processing the daily averages of data collected by the T8 inclinometer probe from October 8, 2000 to April 8, 2003 are depicted in Fig. 11 with respect to time. During this period the in-place inclinometer was removed 4 times to perform the measurements by using the manual probe. It was seen that data collected just after the lowering of the in-place inclinometer into the casing were clearly different from the general pattern of the series, and therefore they were not used in the processing.

In Fig. 11 it is seen that the initial values of the displacement direction are clearly different from the expected value of about 300° (or −60°, anticlockwise from north direction) and eventually tend to it. Accordingly, velocity direction gets a steady pattern close to 300° only after day 719. As the values of acceleration magnitude are as small as not to be significantly different from zero, the estimates of the values of acceleration (both magnitude and direction) cannot be reliable. As a result, the values of acceleration direction are scattered over a wide range and nearly always do not follow any pattern.

The state space model gives estimates of signals μ_A and μ_B with standard deviations of about 0.1 mV, equivalent to 0.01 mm. These standard deviations are one order of magnitude less than those calculated for the mobile inclinometer readings, and therefore accuracies of estimates of displacements from in-place inclinometer data (defined as multiples of the standard

Table 2. Comparison between the Displacements Calculated from Mobile and In-Place Inclinometer Data in the T8 Casing

Interval (days)	Mobile		In-place	
	Magnitude (mm)	Direction (degrees)	Magnitude (mm)	Direction (degrees)
March 15–June 20, 2001	6.283	287	3.287	282
June 20–October 2, 2001	1.622	291	0.398	350
October 2–November 26, 2001	0.945	295	0.059	334
November 26, 2001–March 7, 2002	1.201	238	0.562	329
March 7–July 3, 2002	2.613	318	0.345	334
July 3–October 30, 2002	0.426	336	System out of order	
October 30–December 16, 2002	2.633	300	1.044	335
December 16, 2002–April 8, 2003	1.627	282	1.597	297
April 8–July 10, 2003	0.485	288	System out of order	
July 10–November 5, 2003	0.271	333	0.306	299
November 5, 2003–April 6, 2004	2.054	275	2.261	298
April 6–July 28, 2004	0.858	275	System out of order	
July 28–November 29, 2004	1.296	340	0.554	309

deviation) are also expected to be generally one order of magnitude less than accuracies calculated with the mobile inclinometer readings.

Check on the Automatic Monitoring System

Check operations consist of defining the depth where the in-place inclinometer probes have to be installed, as well as evaluating the reliability of the in-place inclinometer data.

Positions of In-Place Inclinometer Probes

To use the monitoring system as a diagnostic tool for defining the alert and warning conditions, the in-place inclinometer probes should be located at the failure zone where they record the maximum displacements. At this purpose it has to be noted that distances between the wheels of the in-place and mobile inclinometer probes are different, and therefore the maximum displacements cannot be directly evaluated from the mobile inclinometer recordings, but must be evaluated with reference to the actual profiles of casings. These profiles may be established by reducing them to curves passing through the edges, top and bottom, of the mobile inclinometer probe (Fig. 12). For the sake of simplicity, only four points (i.e., three positions of the mobile probe) were taken into account and a third degree polynomial function was assumed to describe the curve. In particular cases (very small displacements) this procedure gave misleading results, hence an analysis by assuming the casing profile to vary as the polygonal of positions of the mobile inclinometer probe was preferred. The probe depths (calculated from the top head at the surface to the middle point of the probe) providing the maximum displacements and obtained by assuming the polygonal profile are reported in Fig. 13 for Inclinometer S4. They were calculated either by maximizing the displacement between two successive mobile inclinometer measurements (current displacement) or by maximizing the displacement accumulated since July 1997. It is seen that the depths evaluated with reference to the current displacements vary between 35.9 and 36.6 m, being close to 36.2 m when current displacements are larger; while depth evaluated with reference to the accumulated displacements is less variable and comprised between 36.15 and 36.45. Accordingly, the middle point of the in-place inclinometer probe was fixed at 36.2 m.

In-Place Inclinometer Recordings

An example of in-place inclinometer recordings is given in Fig. 14 for axes A and B of Inclinometer T8. It includes a period (P1) when the signal was found to be disturbed due to the presence of the amplifier datalogger (at the end of this period it was removed); a period (P2) when the signal is around zero because a lightning strike had damaged the power supply; and eventually a period when the signal looks more accurate, but suffers some shifts indicated by the arrows. The closed arrows indicate the shifts that occurred after mobile inclinometer measurements. It was found that in-place probe removal and its replacement in the casing may cause the signal patterns to shift up to 100 mV. This disturbance is probably caused by an unavoidable small variation of the positions of the probe wheels in the casing. As shown in the enlargement of Fig. 14(b), the shift is not instantaneous: it was found that it may take a time varying from one hour to two weeks. This signal stabilization is likely to be related to the settling of the head assembly and of the wire which the probe is hung with.

The shift indicated by the open arrow in Fig. 14(b) occurred after the performance of a piezometric measurement. It was carried out by using a water level indicator, whose probe and cable passed close to the in-place inclinometer.

Table 3. Displacement Components, Variances, and Triple Standard Deviation from Mobile Inclinometer Recordings

Interval (days)	x (mm)	y (mm)	$s^{2\|k}_{x\|j}$ (mm^2)	$s^{2\|k}_{y\|j}$ (mm^2)	$3s_x$ (mm)	$3s_y$ (mm)
October 30, 2002–December 16, 2002	−2.567	0.572	0.023	0.008	0.460	0.273
December 16, 2002–April 8, 2003	−1.622	−0.125	0.025	0.007	0.471	0.260

Table 4. Displacement Components, Variances, and Triple Standard Deviation from In-Place Inclinometer Recordings

Interval (days)	x (mm)	y (mm)	$s_{\underline{x}}^2\|_j^k$	$s_{\underline{y}}^2\|_j^k$	$3s_{\underline{x}}$ (mm)	$3s_{\underline{y}}$ (mm)
October 30, 2002–December 16, 2002	−0.679	0.768	9×10^{-6}	1.6×10^{-5}	0.009	0.012
December 16, 2000–April 8, 2003	−1.574	0.272	9×10^{-6}	1.6×10^{-5}	0.009	0.012

Simeoni and Mongiovì (2003) classified the disturbances to the signal as four types:

1. Noise due to the acquisition system;
2. Systematic errors associated to damages to the acquisition system or to the probes;
3. Occasional errors due to foreseen or acknowledged external actions, as shifts caused by the removal of the in-place inclinometer probe to perform the mobile inclinometer measurements, or by the performance of piezometric measurements by means of a water level indicator; and
4. Occasional errors due to unforeseen and unknown phenomena.

Although disturbances of Types 1 and 3 are directly introduced in the statistical model defined in Eq. (15) by $\boldsymbol{\varepsilon}_t$ and $\boldsymbol{\lambda}\cdot\mathbf{x}_t$, Simeoni and Mongiovì (2003) suggest to recognize errors of Types 2 and 4 by comparing the estimated displacements from in-place inclinometer data to the changes in the casing profiles at the positions where the in-place inclinometer probes are fixed. The only alternative way to survey the casing profiles is to use the mobile inclinometer probe. Table 2 contains the results obtained for Inclinometer T8. They differ from those reported in Simeoni and Mongiovì (2003) because casing spiral no longer has been taken into account in the data processing. It is seen that usually there is no agreement between in-place and mobile displacements, neither in magnitude nor in direction. Differences in magnitude are often larger than 1 mm, differences in direction may be as large as 90°. It is interesting to note that at the first time interval the mobile inclinometer displacements are twice the in-place inclinometer displacement in magnitude, although the directions are almost the same. This fact was also recognized for the other inclinometers and made it possible to detect a malfunctioning in the amplifier. The amplifier was then removed.

On the contrary, in the time interval December 16, 2002–April 8, 2003 displacement from in-place inclinometer is similar to the mobile one, but directions differ by more than 20°. In order to gain some insight into the comparison between mobile and in-place inclinometer data, a statistical approach has been defined.

Statistical Approach for the Comparison of Data

The changes in the casing profile where the in-place inclinometer probe is fixed are calculated from the mobile inclinometer data by assuming the casing profile to vary as the polygonal of positions of the probe. In Fig. 12 the case of Plane A of Inclinometer T8 is shown. The in-place inclinometer probe is fixed at a depth of 24.3 m with respect to the middle point between the wheels, meanwhile the measurements by the mobile inclinometer probe are made at 0.5 m intervals. The value of the change of A corresponding to the length of the in-place inclinometer probe, between measurements j and k: $\bar{A}_{ip}|_j^k$, may be expressed as

$$\bar{A}_{ip}|_j^k = a\bar{A}_{24}|_j^k + \bar{A}_{24.5}|_j^k + b\bar{A}_{25}|_j^k \tag{16}$$

According to Eqs. (4a) and (10a) $\bar{A}_{ip}|_j^k$ is a linear combination of normally distributed variables, and its variance is expressed by

$$s_{A_{ip}}^2|_j^k = (a^2 + 1 + b^2)s_A^2|_j^k \tag{17}$$

In the same way, $\bar{B}_{ip}|_j^k$ and $s_{B_{ip}}^2|_j^k$ may be written as

$$\bar{B}_{ip}|_j^k = c\,\bar{B}_{24}|_j^k + \bar{B}_{24.5}|_j^k + d\,\bar{B}_{25}|_j^k \tag{18}$$

$$s_{B_{ip}}^2|_j^k = (c^2 + 1 + d^2)s_B^2|_j^k \tag{19}$$

By defining the components of displacements as

$$x = -\bar{B}_{ip}|_j^k \frac{D}{K} \tag{20}$$

$$y = -\bar{A}_{ip}|_j^k \frac{D}{K} \tag{21}$$

(x and y are positive along Axes A_{180} and B_{180}, respectively) their variances are

$$s_x^2|_j^k = \left(\frac{D}{K}\right)^2 s_{B_{ip}}^2|_j^k \tag{22}$$

$$s_y^2|_j^k = \left(\frac{D}{K}\right)^2 s_{A_{ip}}^2|_j^k \tag{23}$$

The results obtained by processing the data from the two time intervals October 30–December 16, 2002 (668–715 days since January 1, 2001) and December 16, 2002–April 8, 2003 (715–828 days since January 1, 2001) are reported in Table 3.

The data collected by the in-place inclinometer during the same time intervals are reported in Fig. 14(b). As mentioned in paragraph 5.2 they include some shifts due to the performance of either mobile inclinometer or water level measurements. These data have been processed by using the model defined in Eq. (15) and results of displacements, velocity, and acceleration are those reported in Fig. 11. Values of components of displacements, variance and three times the standard deviation are listed in Table 4. The quantities relative to the in-place inclinometer are reported with the underscore in order to distinguish them from those relative to the mobile inclinometer.

In attempting to decide if difference of values between mobile and in-place inclinometer are due to the accuracy of measurements, we can formulate the null hypotheses H_{0x} and H_{0y}

$$H_{0x}: x = \underline{x}, \quad H_{0y}: y = \underline{y} \tag{24}$$

Table 5. Standardized Variables z_x and z_y and Critical z Score for Two-Tailed Test

Interval (days)	z_x	z_y	$z_{5\%}$	$z_{1\%}$	$z_{0.1\%}$
October 30, 2002–December 16, 2002	−12.31	−2.15	−1.96	−2.58	−3.29
December 16, 2002–April 8, 2003	−0.30	−4.58	−1.96	−2.58	−3.29

Table 6. Confidence Interval for Components of Displacement x and y

Interval (days)	Confidence interval for x			Confidence interval for y		
	95%	99%	99.9%	95%	99%	99.9%
October 30, 2002–December 16, 2002	(−2.867) to (−2.266)	(−2.961) to (−2.172)	(−3.071) to (−2.062)	(0.393) to (0.751)	(0.337) to (0.807)	(0.272) to (0.872)
December 16, 2002–April 8, 2003	(−1.929) to (−1.314)	(−2.026) to (−1.217)	(−2.138) to (−1.105)	(−0.294) to (0.045)	(−0.348) to (0.098)	(−0.410) to (0.160)

versus the alternative hypotheses

$$H_{1x}: x \neq x, \quad H_{1y}: y \neq y \tag{25}$$

The corresponding standardized variables are given by

$$z_x = \frac{x - \underline{x}}{s_{x\underline{x}}}, \quad z_y = \frac{y - \underline{y}}{s_{y\underline{y}}} \tag{26}$$

with variances $s^2_{x\underline{x}}$ and $s^2_{y\underline{y}}$ equal to

$$s^2_{x\underline{x}} = s^2_x|^2_1 + s^2_{\underline{x}}|^2_1 \cong s^2_x|^2_1 \tag{27a}$$

$$s^2_{y\underline{y}} = s^2_y|^2_1 + s^2_{\underline{y}}|^2_1 \cong s^2_y|^2_1 \tag{27b}$$

The values of the variables for the inclinometer data and their critical values for two-tailed test at levels of significance equal to 5, 1, and 0.1% are shown in Table 5.

For the time interval October 30–December 16, 2002 the hypothesis H_{0x} is rejected at any value of the level of significance; meanwhile the hypothesis H_{0y} is rejected at 5% the significant level. For the time interval December 16, 2002–April 8, 2003 the hypothesis H_{0x} is never rejected; while hypothesis H_{0y} is rejected at all levels of significance.

It is worth noting that when the hypothesis H_0 is rejected for the component x of displacement, that usually is the largest component, the value of direction differ significantly from the expected one (Table 2). The expected direction is the direction of the displacements calculated by using the mobile inclinometer recordings and accumulated since July 1997. As the magnitude of the accumulated displacements is bigger than the magnitude of the current displacements, the accuracy of the expected direction should be small (Fig. 9). For Inclinometer T8 the expected value of direction ranges between 293 and 322°. For the time interval October 30–December 16, 2002, where the hypothesis H_0 is rejected for the component x, the direction calculated with the in-place inclinometer data is equal to 335° and differs significantly from the expected direction 293–322°. For the time interval December 16, 2002–April 8, 2003 days the direction from in-place data is 297° and falls inside the expected interval.

As the variances of components x and y are some orders of magnitude less than variances of components x and y, the comparison between components of displacement may be done just verifying if components $\underline{x}$ and $\underline{y}$ fall inside or outside the confidence intervals of components x and y. The 95, 99, and 99.9% confidence intervals for the time intervals October 30–December 16, 2002 and December 16, 2002–April 8, 2003 are shown in Table 6. It is seen that when the null hypothesis H_0 was rejected the component of the in-place inclinometer displacement falls outside the confidence interval of the component of the mobile displacement.

In Table 7 discrepancies in displacement, either for magnitude or direction, are compared to the accuracy of magnitude and direction of displacements calculated from the mobile inclinometer readings. Accuracy was evaluated by using Eqs. (13) and (14) in which $s_A|^k_j$ and $s_B|^k_j$ were evaluated by multiplying the standard deviations calculated according to Eqs. (17) and (19) for the confidence coefficients 1.96, 2.58, and 3.29 relative to the 95, 99, and 99.9% confidence intervals, respectively. For the first time interval, when hypothesis H_0 was always rejected for component x, both discrepancy in magnitude and in direction are bigger than the accuracy. For the second time interval, when hypothesis H_0 was rejected for component y, only the discrepancy in direction is bigger than accuracy. Therefore, it may be argued that direction of displacement represents a good indicator to check the reliability of displacements.

Origin of Errors

The comparison between mobile and in-place inclinometer displacements make it possible to recognize the discrepancies between the two types of measurements, and not to state if both of them or which one are reliable. Nevertheless, if displacements or components of displacements calculated from the two types of measurements do not differ by using the statistical approach, it is likely that both types of measurements are correct; on the contrary, if discrepancies have been recognized, at least one type of measurement has to be affected by error or disturbance. With reference to the classification of disturbances made in paragraph 5.2, the discrepancies in displacements evaluated for the time intervals October 30–December 16, 2002 and December 16, 2002–April 8, 2003 could be associated with disturbances of type 4 in the signal of the in-place inclinometer. Actually, this may be the case for the time interval October 30–December 16, 2002,

Table 7. Discrepancies in Mobile and In-Place Displacements and Accuracy of Displacements from Mobile Inclinometer Recordings

Interval (days)	Discrepancy		Accuracy of displacement magnitude (mm)			Accuracy of displacement direction (degrees)		
	$\lvert\Delta d\rvert$ (mm)	$\lvert\Delta\theta\rvert$ (°)	95%	99%	99.9%	95%	99%	99.9%
October 30, 2002–December 16, 2002	1.589	35	0.332	0.436	0.558	5	7	9
December 16, 2002–April 8, 2003	0.030	15	0.320	0.420	0.537	7	9	11

when on day 697 the piezometric measurement was carried out by lowering a water level indicator in the casing and passing the in-place inclinometer. It is likely that the insertion of the water level indicator made the in-place inclinometer move and the signal drift. But, as a matter of fact, on that day Signals A and B of the in-place inclinometer also started to accelerate.

During the second time interval (December 16, 2002–April 8, 2003), the discrepancy is between the components y and $\underline{y}$, that are smaller than components x and $\underline{x}$. In this period neither anomaly cannot be recognized in the signals of the in-place inclinometer nor piezometric or manual inclinometer measurements were performed. Therefore, disturbances on Signal A may be caused either by the replacement of the inclinometer after the manual measurements on day 715 or by the assumptions made in the processing of mobile inclinometer recordings. In particular, the data were always processed by assuming relationships (3) to be valid even though the systematic errors ε_{Ai}^{s} and ε_{Bi}^{s} can change when the probe is turned on the opposite groove. If this is the case they cannot be deleted by using Eq. (2) and the bias-shift error is introduced (Mikkelsen 2003). Further, three types of systematic errors were recognized by Mikkelsen (2003): the sensitivity drift, the rotation error, and the depth positioning error. Following the methods suggested by Mikkelsen (2003), the bias-shift error and the rotation error were estimated to know if they could be responsible for the discrepancy between mobile and in-place inclinometer displacements. The sensitivity drift and the depth positioning error were assumed to be null. The former because it was not detected during the probe calibration, the latter because changes in the axial length of the casing, changes in the cable length, or changes of the top reference mark were not likely to occur owing to the small displacements and the care given during the measurements. As expected, the bias-shift and the rotation errors were small as they were summed on two intervals only. For the time interval December 16, 2002–April 8, 2003 a cumulative error of +0.024 mm was estimated for the component y. This value is not big enough for accepting hypothesis H_{0y}.

Moreover, mobile and in-place measurements were processed by assuming a linear fitting of the calibration data without taking account for errors due to linearity. These errors could be significant in the time interval December 16, 2002–April 8, 2003, and could be the reason of their discrepancy in size. A reduction of the errors due to linearity could be achieved by using smaller ranges of calibration similar to the inclination intervals measured in the field. Further errors in the assessment of the displacements from mobile recordings could be included when a polygonal was assumed to describe the casing profile. It may be that these errors are more significant when the displacements are small.

Concluding Remarks

With 4 years experience of real-time monitoring of landslide displacements it is useful to highlight some important aspects that govern the way the monitoring system has been managed and the data have been processed. Even though the landslide has so far moved intermittently with small and slow displacements, an accelerated phase of movement resulting from exceptional rainfall events or a progressive failure phenomenon can be expected. The hazard related to such kind of movement and the presence of some of the most important transport and communication lines through the Alps requires the use of an alarm and warning system based on the monitoring of displacements and a landslide evolution model.

Any technical device is never infallible so it is good practice to not depend on only one type of instrument or technique. For the Castelrotto landslide the simplest system was to combine in-place inclinometers with periodical measurements by using a mobile probe. In this way, it was possible to detect the position of the sliding surface and to place only one in-place inclinometer in each casing. Besides, periodical measurements by using the mobile probe provided the casing profile at any depth, and gave useful data for checking the reliability of the displacements evaluated from the in-place inclinometer recordings. In fact, if monitoring data have to be used for defining the mechanism of a landslide and then for managing a warning system the geotechnical engineer is asked to check the functioning of the system and assess the reliability of data.

The need to monitor the landslide movements during a possible acceleration, that means to monitor large displacements, demanded the use of inclinometer sensors with a wide range and, therefore, with a high value of accuracy. Consequently, when the displacements were small in magnitude the variation of signal was on par with the level of accuracy of the instrument. In such condition the signal of the in-place inclinometer and the recordings of the mobile probe could be processed only by using a statistical approach.

The statistical approach first estimated the best value of measures and their accuracy by analyzing the checksums of the mobile recordings and by using a LQTM to process the automatic readings. The LQTM was also helpful for estimating the kinematic characteristics of the movement. Given the best values of measures, the approach compared the displacements evaluated from periodical and automatic measures with the purpose of assessing the reliability of real-time and periodical measurements. It was seen that the comparison by using a statistical test between directions of displacements from in-place inclinometer data or mobile probe recordings represents an easily assessed and good indicator to check the reliability of displacements. Nevertheless, further studies should be made for investigating the influence of the calibration curve and of the polygonal used for the casing profile on the smallest displacements.

Acknowledgments

The writers are grateful to Mr. Marco Bragagna for performing the manual inclinometer measurements since 1997 and Dr. Enrico Pellizzaro for his help with the data processing.

References

Bhandari, R. K. (1988). "Special lecture: Some practical lessons in the investigation and field monitoring of landslides." *Proc., 5th Symp. on Landslides*, Lausanne, Vol. 3, 1435–1457.

Cooper, M. R. (2000). "Presentation of monitoring data for unstable slopes." *Proc., 8th Symp. on Landslides*, Cardiff, U.K., 311–316.

Cruden, D. M., and Varnes, D. J. (1994). "Landslides types and processes." *Landslides: Investigation and mitigation*, Transportation Research Board. National Academy of Sciences, Washington, D.C., 36–75.

Doornik, J. A. (1998). *Object-oriented matrix programming using ox 2.0*, Timberlake Consultants, London.

Dunnicliff, J. (1993). *Geotechnical instrumentation for monitoring field performance*, Wiley, New York.

Koopman, S. J., Shepard, N., and Doornik, J. A. (1999). "Statistical algorithms for models in state space using SsfPack 2.2." *Econom. J.*, 2, 113–166.

Mikkelsen, P. E. (2003). "Advances in inclinometer data analysis." *Proc., 6th Int. Symp. on Field Measurements in Geomechanics*, Oslo, Norway, 555–567.

Simeoni, L. and Mongiovì, L. (2003). "The problematic management of the displacement monitoring system of a landslide." *Proc., 6th Int. Symp. on Field Measurements in Geomechanics*, Oslo, Norway, 673–680.

Simeoni, L., Proietti, T., and Mongiovì, L. (2003). "Analysis and prediction of slow landslide evolutions by using automatic displacement monitoring systems—Technology roadmap for rock mechanics." *Proc., Int. Symp. on Rock Mechanics*, Sandton, South Africa, 1077–1082.

Taylor, J. R. (1986). *Introduzione all'analisi degli errori*, Zanichelli, Bologna, viii–223 (in Italian).